coatings

MDPI

Article

Microstructure and Wear Performance of High-Velocity Arc Sprayed FeMnCrNiBNbAl Coating

Wenhui Qiang, Min Kang *, Jitao Liu and Joseph Ndiithi Ndumia

College of Engineering, Nanjing Agricultural University, Nanjing 210031, China; 2022812040@stu.njau.edu.cn (W.Q.); 2020212004@stu.njau.edu.cn (J.L.); ndiithindumia@gmail.com (J.N.N.)
* Correspondence: kangmin@njau.edu.cn

Abstract: In this study, FeMnCrNiBNbAl wear-resistant coatings were prepared via high-velocity arc spraying technology on the surface of Q235 steel. The effects of spraying distance, voltage, and current on the coating performance were studied via the orthogonal experimental method with microhardness and porosity as evaluation indicators, and the process parameters were optimized. The order of primary and secondary factors affecting coating performance were: spraying distance, voltage, and current. The optimized process parameters are: spraying distance 200 mm, voltage 36 V, and current 240 A. The coating prepared using the optimized process parameters has an average microhardness of 756 HV0.1 and an average porosity of 1.03%. The coating mainly consists of α-Fe, Fe-Cr, Ni-Cr-Fe, Al_2O_3, and (Fe, Ni) solid solution. The coating friction coefficient was 0.5 while that of the substrate was 0.7. The depth and width of the wear marks of the coating were 6.32 μm and 555.41 μm, respectively, which are 66% and 32% lower in comparison with Q235 steel under the same test conditions. The wear forms of this coating were mainly fatigue peeling and adhesive wear.

Keywords: high-velocity arc spraying; FeMnCrNiBNbAl coating; microstructure; microhardness; wear mechanism

Citation: Qiang, W.; Kang, M.; Liu, J.; Ndumia, J.N. Microstructure and Wear Performance of High-Velocity Arc Sprayed FeMnCrNiBNbAl Coating. *Coatings* **2024**, *14*, 428. https://doi.org/10.3390/coatings14040428

Academic Editor: Philipp Vladimirovich Kiryukhantsev-Korneev

Received: 14 March 2024
Revised: 31 March 2024
Accepted: 1 April 2024
Published: 2 April 2024

1. Introduction

Shaft components, as important components for transmitting motion and power, play an important role in achieving rotational motion and torque transmission. One of the main forms of failure is wear, which not only causes component failure but also increases maintenance costs [1,2]. Remanufacturing technology has the function of repairing scrapped parts. The repaired parts can be used as new products, greatly reducing resource waste and benefiting economic development. Therefore, using remanufacturing technology to repair the damaged shaft components that have failed due to wear can not only restore their original functions, or even better than the original function, but also decrease costs and increase economic efficiency [3].

As a remanufacturing technology suitable for industrial fields, high-velocity arc spraying (HVAS) possesses the characteristics of energy saving, low cost, and high efficiency. The main principle is that the two cored wires are linked with the positive and negative terminals of the power supply. When they contact each other and short circuit, the high temperature melts the cored wires, and the molten droplets are atomized by high-pressure air to form a coating on the substrate [4,5]. Commonly used coatings are Fe-based, Co-based, Ni-based, etc. Among them, iron-based coatings have become a research hotspot and have been broadly used in the surface repair and remanufacturing of various parts owing to their low cost and good mechanical properties. Tian et al. [6] used high-velocity arc spraying technology to prepare FeNiCrAl coating, and found that a dense layer of Al_2O_3, Fe_3Al and iron oxides formed on the surface of the coating resulted in higher hardness and better wear resistance. Zhang et al. [7] prepared FeCrNiNbBSiW coating by HVAS technology, and found that the coating had low porosity and high-temperature oxidation

resistance. Ding et al. [8] used the HVAS method to make FeCrNi/CBN composite coating on 45 steel. The coating has high bonding strength and average microhardness, which are 30.5 MPa and 580 HV0.1, respectively. Studies have shown that the chemical composition of the coating directly affects the coating performance [9]. To enhance the wear resistance of the Fe-based coating, Son et al. [10] added B and C elements to the iron-based coating. The research results showed that the coating contained $(Cr, Fe)_2B$ borides, which increased the hardness, corrosion resistance, and wear resistance of the coating by two to five times over that of stainless steel. Cheng et al. [11] prepared FeBSiNb coating by a wire arc spraying process and added B and Nb elements to the iron-based cored wire. The wear resistance was about three times higher than that of 3Cr13 coating. Pokhmurskii et al. [12] prepared an alloy coating in which a limited quantity of B, Ni, Mn and other elements were added to FeCrAl powder core, and found that hard particle oxides and borides were precipitated in the coating at high temperature, thus enhancing the wear resistance of the coating. The above studies show that by adding an appropriate quantity of alloy elements powder to the Fe-based cored wire, the coating can perform better in terms of higher hardness, wear resistance, and oxidation resistance, which play a critical role in enhancing the coating quality.

Previously, our research group studied the microstructure and wear resistance of FeMnCrNi coating, and obtained a hardness of 353.44 HV0.1 [3], which is 1.72 times that of Q235 steel. Moreover, under the loading of 4 N to 8 N, the wear rate of FeMnCrNi coating increased from 14.126×10^{-6} to 21.985×10^{-6} $mm^3/N{\cdot}m$, whereas the wear rate of Q235 steel increases from 19.129×10^{-6} to 39.584×10^{-6} $mm^3/N{\cdot}m$. Although FeMnCrNi coating has certain advantages in hardness and friction and wear performance compared with Q235 steel matrix, as a wear-resistant coating for shaft parts, it is obvious that the hardness and wear resistance of FeMnCrNi coating is not good enough. Therefore, in this experiment, on the basis of FeMnCrNi cored system, B, Nb, and Al alloy elements powder were added, and the FeMnCrNiBNbAl coating was prepared on Q235 steel substrate by HVAS technology. The influence of distinct process parameters on coating properties, such as spraying distance, voltage, and current, were studied by the orthogonal test method to determine the optimized process parameters. The morphology and properties of the coating were characterized under optimized process parameters in order to prepare a wear-resistant coating with excellent comprehensive properties on the substrate surface. The conclusion of this research provides a basis for the further study of shaft component repair and remanufacture.

2. Experimental Materials and Methods

2.1. Experimental Materials and Coating Preparation

This experiment used a self-designed FeMnCrNiBNbAl powder cored wire as the spraying material, with a diameter of 2 mm and a filling rate of 30%~32%. The specific composition is shown in Table 1 and the coating sample is shown in Figure 1. The substrate material was Q235 steel, which is commonly used in shaft parts. Before arc spraying, the surface of the substrate material was cleaned with anhydrous ethanol, and then the substrate was sandblasted using grit blasting equipment (LS1313FK-A; Liangshi, Shanghai, China) as shown in Figure 2 to decontaminate, remove rust, and roughen the surface. The sandblasting was performed using 16 mesh white alumina, with a sandblasting pressure of 0.6 MPa and a sandblasting angle of 60°~90°. An electric arc spraying device (LSARC500S; Shanghai Liangshi Co. Ltd., Shanghai, China) as shown in Figure 3 was used for coating preparation.

Table 1. Composition and content of powder core wire (mass fraction, wt%).

Cored Wire	Mn	Cr	Ni	B	Nb	Al	Fe
FeMnCrNiBNbAl	15	10	7	5	6	7	Bal.

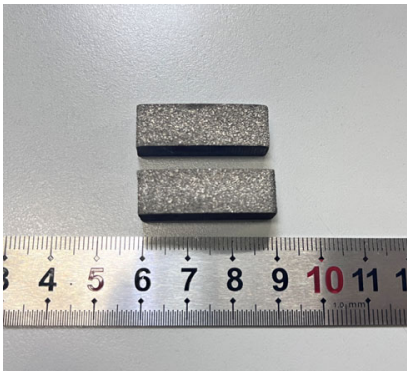

Figure 1. The coating sample.

Figure 2. LS1313FK-A Cyclone Separating Pressure Feeding Box Sandblasting Machine.

Figure 3. LSARC500S type arc melting spray spraying machine.

2.2. Orthogonal Test

This experiment optimizes the spraying distance, voltage, and current as the main parameters for the preparation process of FeMnCrNiBNbAl coating. Through the analysis of

preliminary experimental results, the appropriate parameter range was determined. The experiment was conducted in accordance with the orthogonal test table of three factors and three levels. The specific factor levels of the orthogonal test table are shown in Table 2. Other spraying parameters include: spraying angle of 90° and primary gas pressure of 0.6 MPa.

Table 2. Orthogonal test factor level table.

Levels	Factors		
	A, Voltage/V	B, Current/A	C, Spraying Distance/mm
1	32	160	150
2	36	200	200
3	40	240	250

2.3. Testing Experiments

The FEG250 scanning electron microscope (SEM; Thermo Fischer Scientific, Waltham, MA, USA) was used to analyze the cross-sectional and surface morphology of FeMnCrNiBNbAl coatings. ImageJ software (v.1.52a) was applied to measure the porosity of the coating using the grayscale method by selecting 10 areas on the coating cross-section then averaging the values of the results obtained. The hardness of the coating cross-section was measured using a Vickers indenter tester (Duramin-40; Struers, Ballerup, Denmark), and three sets of data were measured to give the average value. Each set of data measured 10 points for the coating hardness and 5 points for the substrate hardness, and each set of data was collected equidistant from top to bottom. The testing load was 100 g and the loading time was 15 s. The crystal phase structure of the coating was determined using X'PertPowder XRD device (Malvern Panalytical, Malvern, Worcestershire, UK), with measurement parameters of Cu target and X-ray wavelength λ = 0.15406 nm, with a step size of 0.02°, and a scanning angle of 10°~90°. The friction and wear tests were conducted using a ball-on-disk wear tester (CFT-1 tester, ZKKH Technology, Lanzhou, China). The surface of the workpiece was polished in advance to ensure a uniform surface finish. The wear test was performed at normal temperature, no lubrication, and using a counterbody made of an Si_3N_4 ceramic ball with a diameter of 4 mm. The high-velocity linear reciprocating wear form was used, with a test load of 4 N, a reciprocating speed of 900 t/min, a test time of 30 min, and a scratch length of 2 mm. A laser confocal microscope (LEXT OLS 4100, Olympus, Tokyo, Japan) was applied to observe the three-dimensional morphology of wear marks on the surface of the coating and to obtain the size parameters of the wear marks. Energy dispersive spectroscopy (EDS; Bruker, Mannheim, Germany) was applied to mark the chemical elements in different areas of the coating after friction and wear. The wear rate (W_r) of the coating was used to characterize the wear resistance of the coating, and is calculated by the following formula:

$$W_r = \frac{s_s \cdot L_1}{F \cdot L_2} \quad (1)$$

where S_s is the cross-sectional area of the wear scar (mm^2), F is the normal load (N), L_1 is the reciprocating length (mm), and L_2 is the sliding distance (m).

3. Results and Discussion

3.1. Orthogonal Test Results

Microhardness and porosity are important indicators for measuring the wear and corrosion resistance of coatings, which affect the service life of coatings [13]. Therefore, microhardness and porosity are known as evaluation indicators. In order to study the comprehensive performance of coatings and optimize process parameters, the range analysis method was used to weight the microhardness and porosity of coatings, thereby converting multiple indicators into a single comprehensive indicator. The equation for counting the comprehensive weighted score value is as follows:

$$Y_i = a_{i1}b_{i1} + a_{i2}b_{i2} + \ldots + a_{ij}b_{ij} \quad (2)$$

where a is the weighting coefficient, representing the weight proportion of each indicator in the comprehensive score, b is the experimental indicator, and the subscript i and j represent the j-th indicator of the i-th group of experiments. The variation range, K, of experimental indicators (porosity, microhardness) is calculated as follows:

$$K_1 = 1.98 - 0.92 = 1.06 \quad (3)$$

$$K_2 = 738.61 - 639.10 = 99.51 \quad (4)$$

where K_1 represents the variation range in porosity, and K_2 represents the variation range in microhardness.

A comprehensive score of 100 points was assigned, which includes a porosity score of 50 and a microhardness score of 50. For the value of the weighting coefficient a, the actual application of the test indicators should be considered. Higher porosity causes deterioration in the coating properties, and thus the weighting coefficient is negative. The higher the microhardness value, the better the wear resistance of the coating, and thus the weighting coefficient is positive. The weighting coefficient is given by:

$$a_{i1} = -50/K_1 = -47.17 \quad (5)$$

$$a_{i2} = 50/K_2 = 0.50 \quad (6)$$

where a_{i1} is the weighting coefficient of porosity, and a_{i2} is the weighting coefficient of microhardness.

In summary, the formula for the comprehensive performance score Y of this experiment can be obtained by:

$$Y_i = -47.17b_{i1} + 0.50b_{i2} \quad (7)$$

The results of optimizing the comprehensive score of FeMnCrNiBNbAl coating by using the range method are shown in Table 3.

Table 3. Orthogonal test results and comprehensive evaluations.

No.	A, Voltage/V	B, Current/A	C, Spraying Distance/mm	Porosity/%	Microhardness/ HV0.1	Comprehensive Score
1	32	160	150	1.58	680.06	265.50
2	32	200	200	1.15	690.91	291.21
3	32	240	250	1.98	715.82	264.51
4	36	160	200	0.92	738.61	325.91
5	36	200	250	1.05	691.37	296.16
6	36	240	150	1.39	720.15	294.51
7	40	160	250	1.26	662.34	271.74
8	40	200	150	1.43	639.10	252.10
9	40	240	200	1.24	728.96	306.00
Average 1	273.74	287.72	270.70	...	...	...
Average 2	305.52	279.82	307.70	...	...	...
Average 3	276.61	288.34	277.47	...	...	...
R	31.78	8.52	37.00	...	...	...
Major-minor order	C > A > B					
Optimal combination	A2B3C2					

3.2. Analysis of Test Results

In accordance with the analysis results in Table 3, the horizontal value of each factor (spraying distance, voltage, current) in the orthogonal test was taken as the abscissa, while the average value of the sum of the test results at three different levels of the same factor was taken as the ordinate.

As can be seen from Figure 4a,b, as the voltage gradually increases, the porosity first decreases and then increases, while the microhardness increases first and then decreases.

This is because when the voltage gradually increases from low voltage, the arc temperature increases, the wire powder core can be fully melted, and the molten droplets can be effectively spread when they hit the surface of the substrate, which is conducive to enhancing the quality of the coating [14,15]. When the voltage exceeds 36 V, the droplets are prone to high-temperature oxidation and burning, and after cooling, oxide particles are formed and deposited in the coating, resulting in poor internal bonding of the coating and a decrease in the microhardness of the coating [16,17]. In the high-speed arc spraying process, the wire feeding rate is directly related to the current. The wire feeding rate will increase as the current increases [18,19]. The current primarily affects the performance of the coating through affecting the oxidation time and droplet diameter. Therefore, the current affects the performance of the coating. According to Table 3, it can be noted that the spray distance is the most crucial factor affecting the coating performance in the test range. The spraying distance refers to the distance between the spray gun and the surface of the substrate. After the wire is melted in the arc zone, the droplets are atomized and accelerated by compressed air, and hit the surface of the workpiece to form a coating. The flow speed of compressed air is the largest at the nozzle of the spraying gun, and the speed of the molten droplets is the lowest. As the spraying distance increases, the droplets are gradually accelerated, while the speed of the atomized air flow gradually decreases. When the spraying distance is increased from 150 mm to 200 mm, the droplet hits the surface of the substrate at a higher speed, resulting in better spreading ability of the droplet [20]. When the spraying distance exceeds 200 mm, the droplet flight time in the air becomes longer. As a result, the droplet temperature drops, and the droplet easily oxidizes during flight. This increases the internal defects of the coating, which deteriorates the coating performance [21].

It can be observed from Figure 4c that with the increase of voltage and spraying distance, the coating's comprehensive performance first increases and then decreases. As the current increases, the coating's comprehensive performance first decreases and then increases. According to Table 3, it can be seen that the sequence of primary and secondary factors influencing the comprehensive performance of the coating is obtained through range analysis: spraying distance > voltage > current. The obtained order of A2B3C2 gave the optimized process parameters as voltage of 36 V, current of 240 A, and spraying distance of 200 mm.

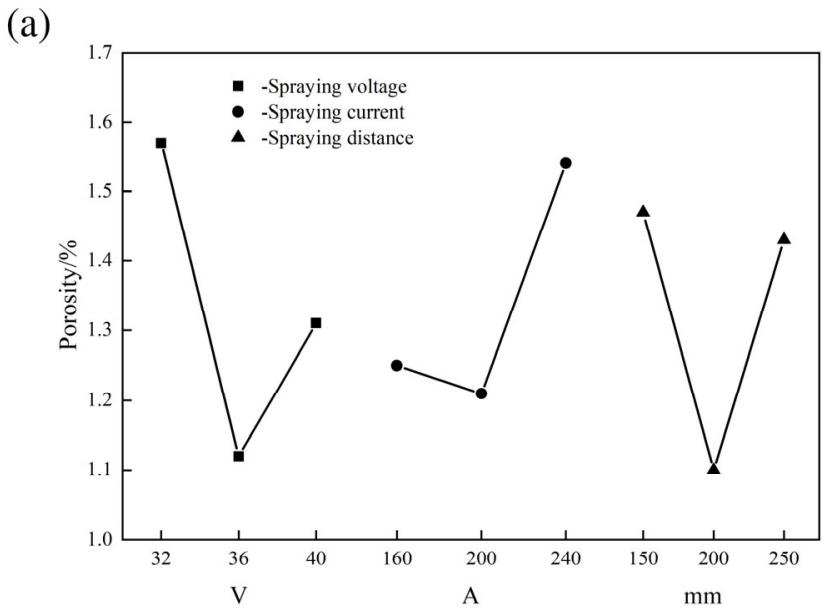

Figure 4. *Cont.*

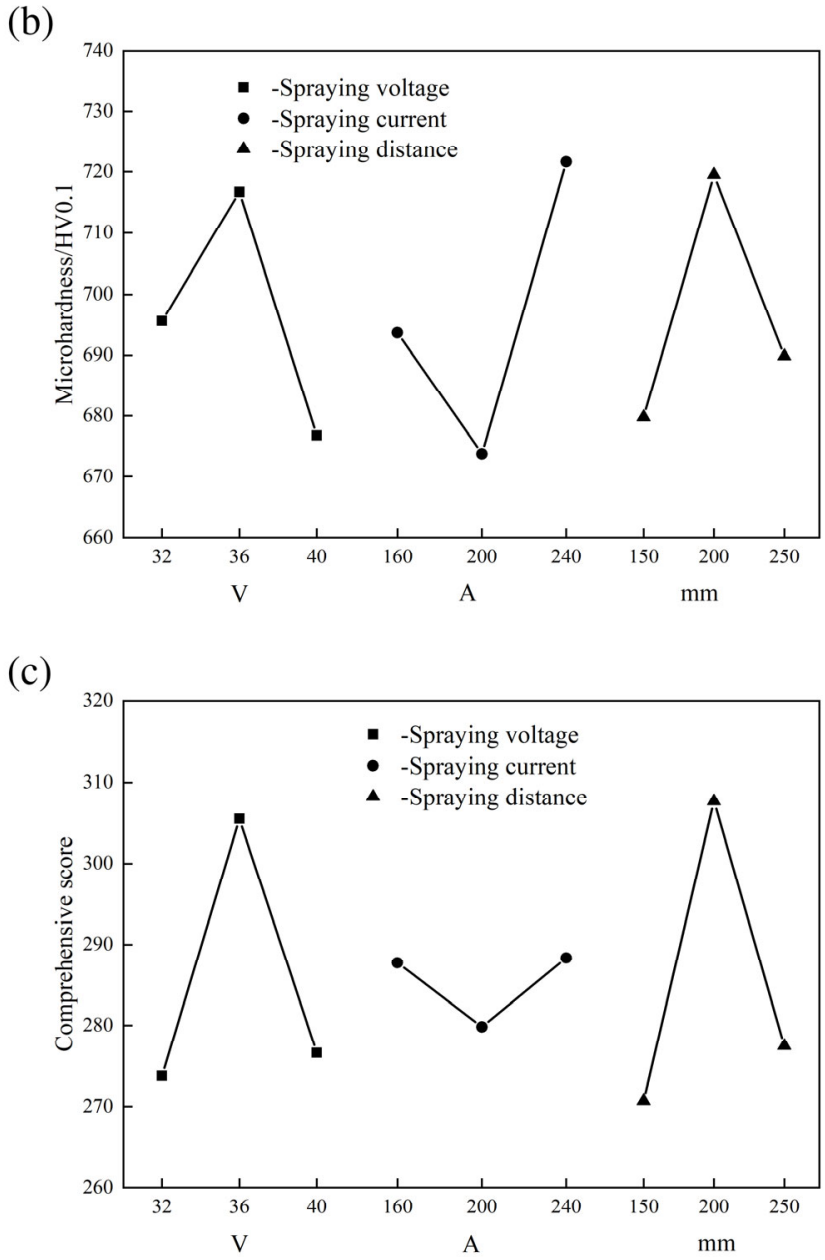

Figure 4. Orthogonal experimental level trend graphs: (**a**) porosity; (**b**) microhardness; (**c**) comprehensive score.

4. Coating Morphology and Performance Characterization Prepared after Optimizing Process Parameters

4.1. Surface and Cross-Sectional Morphology

Figure 5a,b indicates the surface morphology of FeMnCrNiBNbAl coating prepared using the optimized process parameters. From Figure 5a, it can be seen that the coating surface is composed of flattened particles and protruding small particles. No unmelted large particle phase was observed, and a small amount of microcracks emerged on the coating surface. This is because the release of high residual stress can easily cause microcracks in the coating when it cools in the atmosphere [22]. In Figure 5b, it can be seen that the coating surface is mainly composed of flattened particles, semi-molten particles, and pores. The surface of the coating shows an obvious flat region after the spread of molten droplets caused by the high temperature generated by the arc. The powder cored wire melted into a fully molten state, was atomized into micro melt droplets by compressed gas, and spread

into flat particles on the surface of the substrate under the impact of high-velocity airflow. This process was repeated, forming a layered stacked structure.

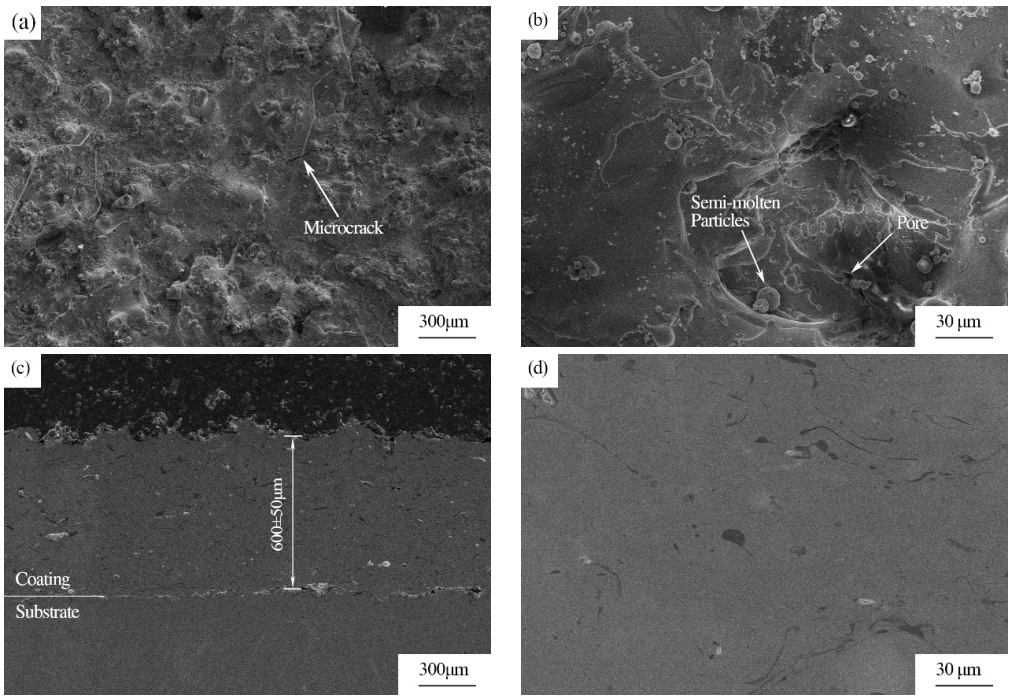

Figure 5. SEM images: (**a**,**b**) the microstructure of the surface; (**c**,**d**) the microstructure of the cross-section.

Figure 5c,d shows the cross-section topography of the coating prepared using the optimized process parameters. It can be observed from the diagram that the coating thickness was uniform with a dense structure, and the coating and the substrate were well combined. After the sandblasting process, an uneven rough surface was formed on the substrate. Molten or semi-molten particles were sprayed onto the surface under the action of compressed air. After condensing and shrinking, the particles interlocked with the rough surface of the substrate, forming a mechanical bond [23]. The molten droplets hit the surface of the substrate at high velocity and spread to solidify and form layers. The subsequent particles repeated this process to continuously stack and deposit, making the coating form a layered structure. The rapid cooling of droplets makes it impossible for gas to escape, resulting in the formation of pores [24]. Also, during the solidification process, particles form internal pores due to cooling shrinkage [25]. Porosity is an important index to measure the performance of coatings [24]. The cross-section images of FeMnCrNiBNbAl coating were processed by ImageJ to give an average porosity of 1.03%.

4.2. Elemental Analysis

Figure 6 shows the surface distribution of each chemical element on the coating surface. According to Figure 6b–i, the elements inside the coating are evenly distributed. The content of each chemical element detected corresponds to the composition and content of powder core wire shown in Table 1. In addition to the elements added in the design of the wire composition, there is also a certain O element in the coating, which is mainly related to the working principle of arc spraying. In the arc spraying process, the partially molten high-temperature particles are in contact with the compressed gas and oxygen in the working environment during flight, and an oxidation reaction occurs. The generated oxides spread out and stack with the particles, cooling and solidifying to form a coating, so there is the presence of O element in the coating. Observe Figure 6a,h. Figure 6a contains a dark region, A; this corresponds to Figure 6h where we find that the dark region A holds a concentration of Al element, where Al_2O_3 is likely to be formed.

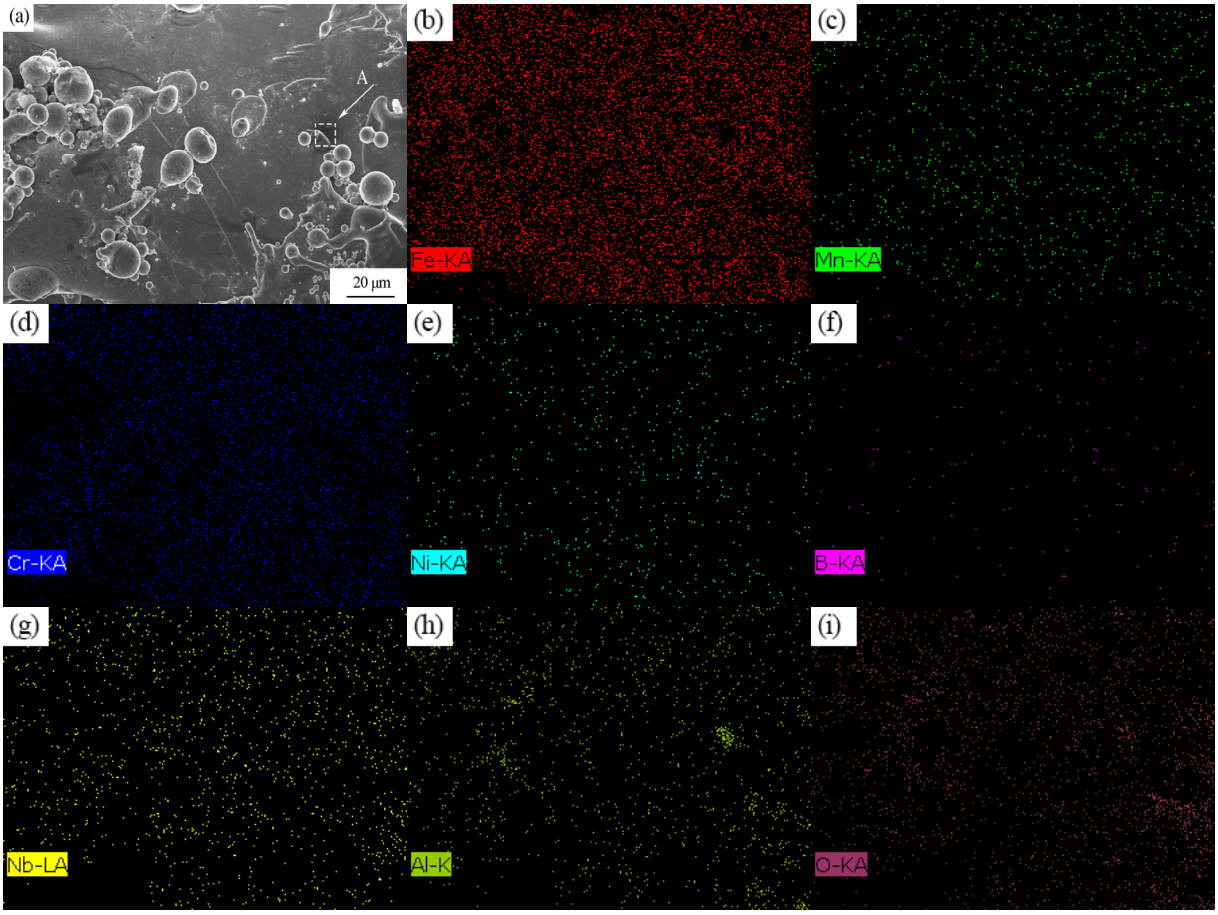

Figure 6. Coating surface element distribution: (**a**) coating surface morphology; (**b**) Fe element; (**c**) Mn element; (**d**) Cr element; (**e**) Ni element; (**f**) B element; (**g**) Nb element; (**h**) Al element; (**i**) O element.

Figure 7 shows the line scan analysis of the intersection area between FeMnCrNiBNbAl coating and Q235 steel section. It can be seen from Figure 7 that the internal structure of the coating is dense and uniform, and the coating is well combined with the matrix. As can be seen from Figure 7b, the element content in the coating region fluctuates along the line scanning direction until becoming stable at the matrix region. There is an obvious transition area at the boundary between coating and matrix, and there is a phenomenon of diffusion of coating elements to matrix.

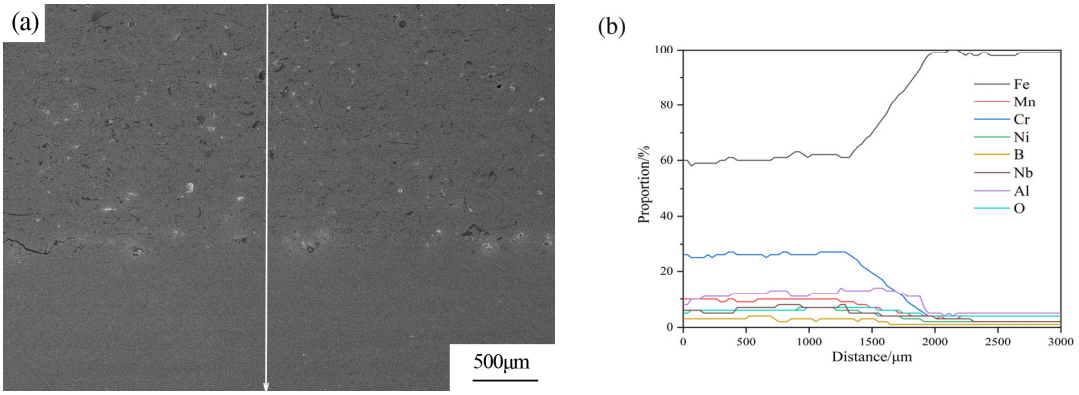

Figure 7. Line scan analysis of FeMnCrNiBNbAl coating section: (**a**) coating cross section morphology; (**b**) line scan analysis.

4.3. XRD Pattern

Figure 8 shows the X-ray diffraction pattern of FeMnCrNiBNbAl coating prepared using the optimized process parameters. The coating primarily consists of α-Fe, Fe-Cr, Ni-Cr-Fe, Al_2O_3, and (Fe, Ni) solid solution. Relevant studies have shown that Cr is an element that promotes the formation of α-Fe [3,26]. Ni-Cr-Fe is a solid solution with high plasticity and toughness, and low hardness [27]. The added Al element is oxidized to produce chemically stable Al_2O_3 during the spraying process [28]. The hard phases of Fe-Cr and (Fe, Ni) solid solution can enhance the hardness and load resistance of the coating and thus improve wear resistance [29].

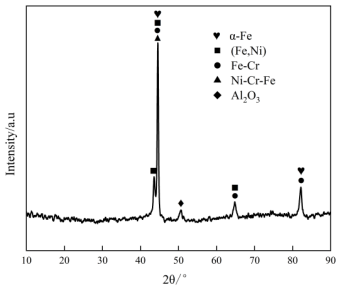

Figure 8. X-ray diffraction pattern.

4.4. Microhardness

Figure 9a is the schematic of hardness indentation and Figure 9b shows the cross-section microhardness distribution curve of FeMnCrNiBNbAl coating prepared using the optimized process parameters. It can be observed from the figure that the coating microhardness is mainly concentrated in the range of 700~800 HV0.1. The average microhardness of the coating is 756 HV0.1, and that of the substrate is about 220 HV0.1. The hardness of the coating is about 3.4 times that of the substrate. Due to the low porosity of the coating, the dispersed oxide and solid solution hard phase result in high hardness and play a role in the dispersion strengthening of the coating [30].

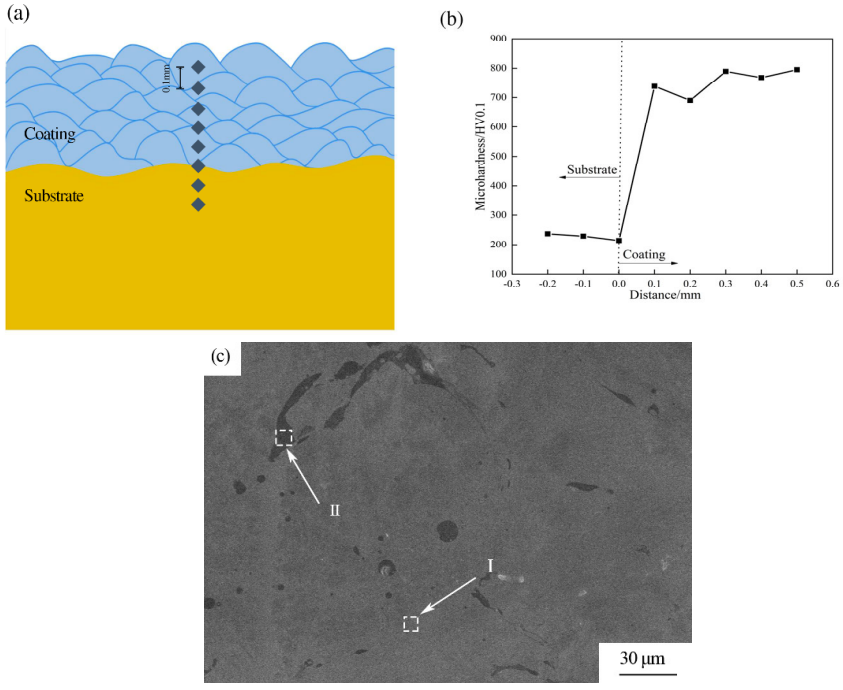

Figure 9. Coating microhardness: (**a**) Schematic of hardness indentation; (**b**) Microhardness variation; (**c**) Micro-zone chemical composition analysis of the coating.

In order to research the reasons for the high hardness of the coating, the micro-components of the coating section were analyzed. It can be seen from Figure 9c that the coating is mainly composed of a large gray area (point I) and dark gray (point II) strip structures. The composition of the micro-regions of these two typical areas were analyzed by EDS. Table 4 shows the mass percentage of the main elements in each micro-region. It can be seen from Table 4 that the gray area contains a large amount of Fe, Cr, and Ni, which is confirmed by XRD analysis. The main phases of the gray area are Fe-Cr and Ni-Cr-Fe. The content of Al and O in the dark gray strip structure in the coating is high, and the content of Fe is low, indicating that the structure is an oxide of Al. The XRD analysis results confirmed the presence of Al_2O_3. At the same time, the structure contains 10.99% C element, indicating the presence of carbides. According to the composition of the coating, the gray area of the coating is mostly Fe-Cr, and the dark gray area is mostly Al_2O_3. The relevant studies show that Al_2O_3 is a high hardness oxide, which is dispersed and embedded in the layered structure, improving the load resistance of the coating. The Fe-Cr solid solution phase in the coating can also improve the coating's microhardness and load resistance.

Table 4. Chemical composition analysis of FeMnCrNiBNbAl coating section.

Zone in Figure 9c	Composition of Main Elements (Mass Fraction/wt.%)								
	O	**C**	**Fe**	**Mn**	**Cr**	**Ni**	**B**	**Nb**	**Al**
I	0.72	9.71	50.92	4.09	13.49	7.30	4.47	7.35	1.95
II	26.86	10.99	8.55	3.75	6.75	1.91	0.27	8.13	32.79

4.5. Wear Performance

Figure 10 shows the friction coefficient curves and the profile of the worn sections of the Q235 steel substrate and FeMnCrNiBNbAl coating. As can be noted from Figure 10a, in the previous stage of friction and wear, the low value of the friction coefficient was due to slippage on the workpiece surface as a result of the low surface roughness after the polishing treatment. Once the friction coefficient curve became stable, the friction coefficient of the coating was about 0.5, and the friction coefficient of the substrate was about 0.7. Compared with the substrate material, the hardness of the counterpart ceramic material Si_3N_4 is higher, and the substrate was cut during the wear process. At a higher friction temperature, the substrate produced a certain adhesion, resulting in a higher friction coefficient of the substrate. Figure 10b and Table 5 show the two-dimensional contour curve of the wear mark and the parameter table of the wear mark sizes of Q235 steel and the coating under the same load and loading time, respectively. It can be noted from the figure that the wear marks of Q235 steel are groove-like, and the middle part is severely worn with dense scratches. The abrasion width of the coating is narrow, relatively flat with fewer scratches. Due to the higher hardness of the coating, the wear resistance of the coating is superior to the substrate. As can be seen from Table 5, the depth, width, and cross-sectional area of the substrate wear marks are 18.81 μm, 816.2 μm, and 7944.54 μm^2, respectively. The width is wider and the wear marks are deeper, mainly because the hardness of the substrate is low, and the grinding ball cuts the substrate surface to form deeper furrows. The depth, width, and cross-sectional area of the coating wear marks are 6.32 μm, 555.41 μm, and 1783.26 μm^2, respectively, and the wear marks are narrower and shallower because the coating has a higher hardness and the surface was not easily cut, thus forming a narrower and shallower groove. Compared with the substrate, the depth, width, and cross-sectional area of the coating are reduced by 66%, 32%, and 78%, respectively, indicating that the coating's wear resistance is obviously better than that of Q235 steel. In addition, under the same working conditions, the average wear rate of the coating is 8.26, whereas the wear rate of the substrate is 36.78, thus the wear rate of the substrate is more than four times that of the coating. This can also indicate that the wear resistance of the coating is much better than that of the substrate.

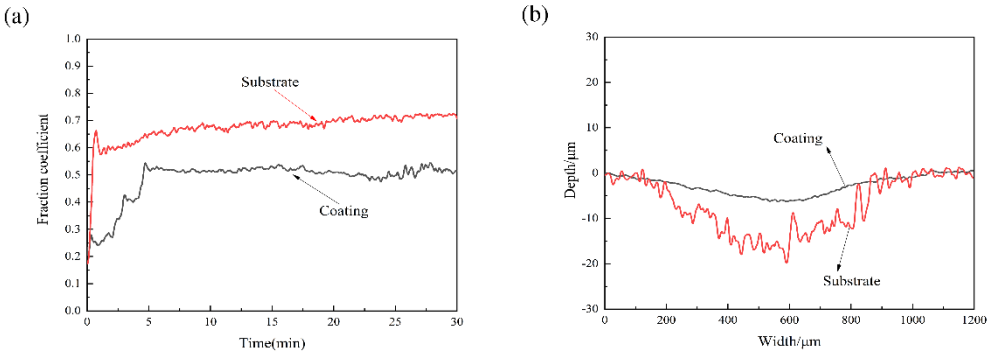

Figure 10. Comparison of wear of coating and substrate: (**a**) friction coefficient curves; (**b**) two-dimensional contour curves of wear scar.

Table 5. Wear scar size parameters.

No.	FeMnCrNiBNbAl				Q235			
	Width/μm	Depth/μm	Cross Section Area/μm^2	Wear Rate/mm^3/N·m	Width/μm	Depth/μm	Cross Section Area/μm^2	Wear Rate/mm^3/N·m
1	547.09	6.76	1731.67	8.02	861.59	19.19	9037.15	41.84
2	554.94	5.13	1605.03	7.43	816.03	16.20	6615.98	30.63
3	564.20	7.06	2013.09	9.32	770.98	21.05	8180.49	37.87
Average value	555.41	6.32	1783.26	8.26	816.20	18.81	7944.54	36.78

Figure 11 shows the wear morphologies of substrate and coating at low and high magnifications. It can be observed from the figure that under the same load and loading time, the wear degree of Q235 is significantly greater than that of the coating. Because the hardness of the counterpart ball is much higher than that of Q235 steel, a large number of grinding chips were generated on the surface during the friction process, and Q235 steel was also cut under the action of load, thus forming a furrow, and its wear form is mainly furrow plastic cutting. The surface of FeMnCrNiBNbAl coating is relatively flat with fewer scratches. There is an obvious fatigue spalling phenomenon and irregular distribution of pits formed after spalling. The mechanism of fatigue spalling of the coating is as follows: firstly, cracks were generated locally containing defects (holes and micro-cracks), and the cracks expanded and extended under the action of high stress. They converged with the surrounding holes to form a long crack resulting in local flaking of the coating, and the flaking debris remained between the friction pair and the coating. Under the load of the friction pair, the coating was constantly squeezed and scraped. The peeling and crack propagation of the coating were further aggravated [17,31]. It can also be seen from Figure 11d that some black areas appeared on the surface of the wear marks. This is because, during the friction process, the friction on the surface of the coating generates a lot of heat and, as a result of this temperature rise, an oxidation reaction of the coating occurs, thus forming an oxide film on the surface. In the initial stage of oxidation, the oxide film protects the coating and reduces the wear rate of the coating. However, with the peeling failure of the coating and the grinding chips rolling between the friction pairs, the oxide film was destroyed, resulting in local peeling. As the wear process progresses, the fresh coated surface exposed by the peeling chips was oxidized into oxide chips. To a certain extent, these oxide chips formed an oxide layer again under friction heat and extrusion, which can improve the coating wear resistance [32]. In the meantime, after chemical element analysis of the worn coating, it was found that some of the peeling areas of the coating contain Si elements. It can be analyzed that during the wear process of the surface of the Si_3N_4 ceramic ball, the fragments of the grinding ball adhere to the coating wear area, and as the grinding ball continues to wear the coating surface, adhesive wear of the coating occurs. Therefore, the wear form of the coating is primarily fatigue peeling and adhesive wear.

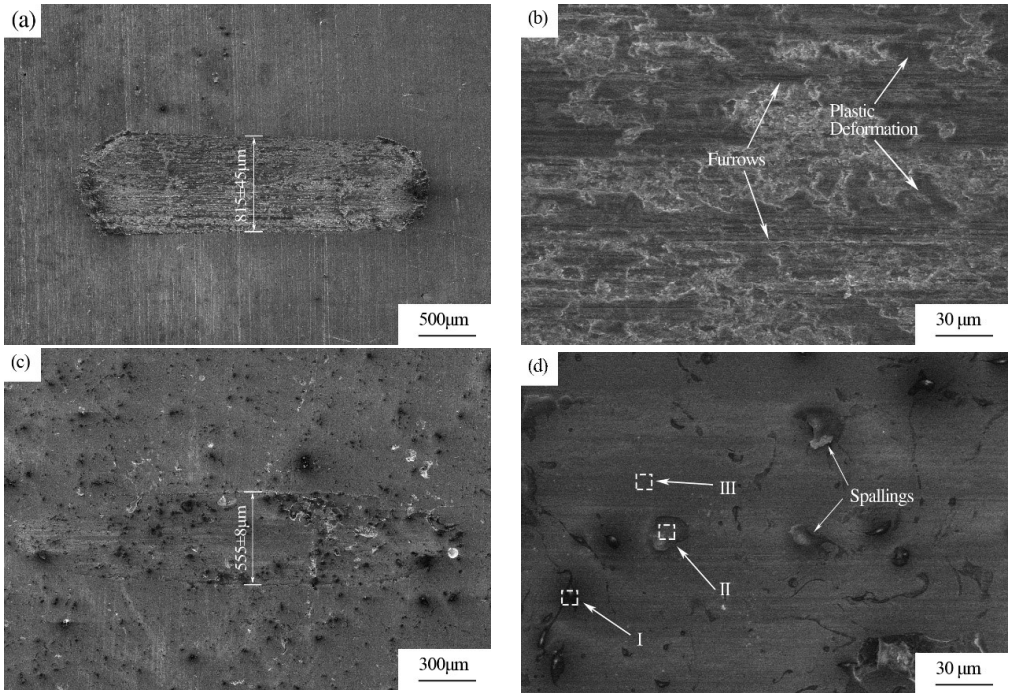

Figure 11. Micro morphology of wear scar of the substrate (**a**,**b**) and coating (**c**,**d**) (I: black convex point; II: gray-white pit; III: gray area).

It was observed that there were a small number of black protrusions I, gray pits II and large gray areas III in the wear marks of the coating. These areas were characterized by their chemical composition. Table 6 shows the content of the main elements in these regions. Al and O elements are mostly found in point I. Combined with XRD results, it can be seen that this point is mainly comprised of Al_2O_3. The hard phase Al_2O_3 is embedded in the coating and plays the role of a supporting "skeleton" for the coating substrate. The hard phase is more susceptible to wear in the initial wear phase. It also hinders the expansion and growth of micro-cracks induced by friction, and effectively enhances the wear resistance of the coating. In point II, there are more O elements with a mass fraction of 42.72%, iron elements with a mass fraction of 31.06%, 8.63% Cr elements and 7.62% Si elements. As the surface of the Si_3N_4 ceramic ball is worn, the fragments of the grinding ball remained in the coating wear area, which may cause oxidation during the friction process. Thus, point II mainly consists of iron oxide, the oxide of Cr and the oxide of Si. Combined with XRD results, point III should be a hard phase containing Fe and Cr.

Table 6. Micro-zone chemical composition analysis of FeMnCrNiBNbAl coating.

Zone in Figure 11d	Composition of Main Elements (Mass Fraction/wt.%)									
	O	**C**	**Si**	**Fe**	**Mn**	**Cr**	**Ni**	**B**	**Nb**	**Al**
I	43.41	—	—	2.94	2.86	6.5	—	—	—	44.29
II	42.72	2.29	7.62	31.06	3.09	8.63	3.2	—	—	1.39
III	0.31	2.77	0.45	62.22	3.72	18.82	7.3	—	2.94	1.47

5. Conclusions

In this study, high-velocity arc spraying technology was applied to make FeMnCrNiBNbAl coating on the surface of Q235 substrate steel. The microstructure, phase composition, and properties (microhardness and wear resistance) of the coating were studied and compared with the substrate. The main conclusions are as follows:

(1) The primary and secondary process parameters affecting the microhardness and porosity of FeMnCrNiBNbAl coating are as follows: spraying distance, voltage, cur-

rent. The optimized process parameters are: voltage 36 V, current 240 A, spraying distance 200 mm.

(2) The performance of FeMnCrNiBNbAl coating prepared using the optimized process parameters is better than that of the orthogonal test group. The microhardness of the coating is mainly concentrated in the range of 700~800 HV0.1, and the average hardness is 756 HV0.1, which is about 3.4 times that of the substrate Q235 steel. The average porosity of the coating is about 1.03%. The coating mainly consists of α-Fe, Fe-Cr, Ni-Cr-Fe, Al_2O_3, and (Fe, Ni) solid solution with a dense and stable microstructure.

(3) The width and depth of the FeMnCrNiBNbAl coating prepared using the optimized process parameters are 555.41 μm and 6.32 μm, respectively. Compared with the substrate, the values decreased by 32% and 66%. The coating's wear resistance is obviously superior to that of Q235 steel. The wear forms of the coating are mainly fatigue peeling and adhesive wear.

Author Contributions: Conceptualization, W.Q.; methodology, W.Q. and M.K.; software, W.Q. and J.L.; validation, J.L. and J.N.N.; formal analysis, W.Q., J.N.N. and J.L.; investigation, J.N.N., M.K. and J.L.; data curation, W.Q. and J.L.; writing—original draft preparation, W.Q.; writing—review and editing, J.N.N.; supervision, J.N.N. and J.L.; project administration, M.K. and J.L.; funding acquisition, M.K. All authors have read and agreed to the published version of the manuscript.

Funding: This present work was supported by Jiangsu provincial Key Research and Development plan (No. BE2020311).

Institutional Review Board Statement: Not applicable.

Informed Consent Statement: Not applicable.

Data Availability Statement: Data are contained within the article.

Conflicts of Interest: The authors declare no conflicts of interest.

References

1. Liu, Z.P.; Zhang, L. A review of failure modes, condition monitoring and fault diagnosis methods for large-scale wind turbine bearings. *Measurement* **2020**, *149*, 107002. [CrossRef]
2. Tian, H.L.; Wei, S.C.; Liang, X.B.; Xu, B.S.; Wang, C.L.; Guo, M.Q.; Tang, Z.H. Bending Fatigue Life and Remanufacturing Benefit Evaluation of High Velocity Arc Spraying Remanufacturing Crankshaft. *Rare Met. Mater. Eng.* **2018**, *47*, 538–545.
3. Liu, J.; Lin, J.; Kang, M.; Ndumia, J.N.; Huang, F. Microstructure and Tribological Properties of Fe-Based Composite Coatings Prepared by High-Velocity Arc Spraying. *J. Therm. Spray Technol.* **2022**, *31*, 644–657. [CrossRef]
4. Amushahi, M.H.; Ashrafizadeh, F.; Shamanian, M. Characterization of boride-rich hardfacing on carbon steel by arc spray and GMAW processes. *Surf. Coatings Technol.* **2010**, *204*, 2723–2728. [CrossRef]
5. Cheng, J.B.; Wang, Z.H.; Xu, B.S. Wear and Corrosion Behaviors of FeCrBSiNbW Amorphous/Nanocrystalline Coating Prepared by Arc Spraying Process. *J. Therm. Spray Technol.* **2012**, *21*, 1025–1031. [CrossRef]
6. Tian, H.L.; Wang, C.L.; Guo, M.Q.; Tang, Z.H.; Wei, S.C.; Xu, B.S. Study of the frictional-wear performance and abrasion resistance mechanism of a high-speed arc-sprayed FeNiCrAl coating. *Surf. Coat. Technol.* **2019**, *370*, 320–330. [CrossRef]
7. Zhang, X.; Wang, Z.H.; Lin, J.R.; Zhou, Z.H. A study on high temperature oxidation behavior of high-velocity arc sprayed Fe-based coatings. *Surf. Coat. Technol.* **2015**, *283*, 255–261. [CrossRef]
8. Ding, P.; Liu, X.J.; Liu, J.J.; Li, J.B.; Li, H.Q.; Zhao, H.Y.; Duan, J.Y.; Jiao, Y.Z. Study on the properties of FeCrNi/CBN composite coating with high velocity arc spraying. *Arab. J. Chem.* **2018**, *11*, 935–941. [CrossRef]
9. Wielage, B.; Pokhmurska, H.; Student, M.; Gvozdeckii, V.; Stupnyckyj, T.; Pokhmurskii, V. Iron-based coatings arc-sprayed with cored wires for applications at elevated temperatures. *Surf. Coat. Technol.* **2013**, *220*, 27–35. [CrossRef]
10. Son, C.Y.; Yoon, T.S.; Lee, S. Correlation of Microstructure with Hardness, Wear Resistance, and Corrosion Resistance of Powder-Injection-Molded Specimens of Fe-Alloy Powders. *Metall. Mater. Trans. A* **2009**, *40*, 1110–1117. [CrossRef]
11. Cheng, J.B.; Liang, X.B.; Wang, Z.H.; Xu, B.S. Microstructure and Mechanical Properties of FeBSiNb Metallic Glass Coatings by Twin Wire Arc Spraying. *J. Therm. Spray Technol.* **2013**, *22*, 471–477. [CrossRef]
12. Pokhmurskii, V.; Student, M.; Gvozdeckii, V.; Stypnutskyy, T.; Student, O.; Wielage, B.; Pokhmurska, H. Arc-Sprayed Iron-Based Coatings for Erosion-Corrosion Protection of Boiler Tubes at Elevated Temperatures. *J. Therm. Spray Technol.* **2013**, *22*, 808–819. [CrossRef]
13. Lin, J.R.; Wang, Z.H.; Lin, P.H.; Cheng, J.B.; Zhang, X.; Hong, S. Microstructure and cavitation erosion behavior of FeNiCrBSiNbW coating prepared by twin wires arc spraying process. *Surf. Coat. Technol.* **2014**, *240*, 432–436. [CrossRef]

14. Newbery, A.P.; Grant, P.S. Large arc voltage fluctuations and droplet formation in electric arc wire spraying. *Powder Metall.* **2003**, *46*, 229–235. [CrossRef]
15. Zhu, W.; Kang, M.; Ndumia, J.N.; Lin, J.; Huang, F.; Zhang, Y. Microstructure and Wear Properties of TiB_2 Reinforced Fe-Based Composite Coating. *J. Mater. Eng. Perform.* **2022**, *31*, 5559–5570. [CrossRef]
16. Buchanan, V.E. Solidification and microstructural characterisation of iron-chromium based hardfaced coatings deposited by SMAW and electric arc spraying. *Surf. Coat. Technol.* **2009**, *203*, 3638–3646. [CrossRef]
17. Gargasas, J.; Valiulis, A.V.; Gedzevicius, I.; Mikaliunas, S.; Nagurnas, S.; Pokhmurska, H. Optimization of the Arc Spraying Process Parameters of the Fe-Base Mn-Si-Cr-Mo-Ni Coatings for the Best Wear Performance. *Mater. Sci.* **2016**, *22*, 20–24. [CrossRef]
18. Ribeiro, R.A.; AssunÇÃO, P.D.C.; Dos Santos, E.B.F.; Braga, E.M.; Gerlich, A.P. Globular-to-Spray Transition in Cold Wire Gas Metal Arc Welding. *Weld. J.* **2021**, *100*, 121–131. [CrossRef]
19. Wu, D.T.; An, Q.; Matsuda, K.; Zhang, Y.G.; Yu, B.J.; Zou, Y. Characteristics of bypass coupling twin-wire indirect arc welding with high-speed welding mode. *J. Mater. Process. Technol.* **2021**, *291*, 11. [CrossRef]
20. Fang, J.C.; Xu, W.J.; Zhao, Z.Y. Arc spray forming. *J. Mater. Process. Technol.* **2005**, *164–165*, 1032–1037. [CrossRef]
21. Zhao, W.-m.; Liu, C.; Dong, L.-x.; Wang, Y. Effects of Arc Spray Process Parameters on Corrosion Resistance of Ti Coatings. *J. Therm. Spray Technol.* **2009**, *18*, 702–707. [CrossRef]
22. Hong, D.; Niu, Y.; Li, H.; Zhong, X.; Tu, W.; Zheng, X.; Sun, J. Comparison of microstructure and tribological properties of plasma-sprayed TiN, TiC and TiB_2 coatings. *Surf. Coat. Technol.* **2019**, *374*, 181–188. [CrossRef]
23. Guo, H.F.; Tian, Z.J.; Huang, Y.H. Laser surface remelting of WC–12Co coating: Finite element simulations and experimental analyses. *Mater. Sci. Technol.* **2016**, *32*, 813–822. [CrossRef]
24. Abbas, R.A.; Ajeel, S.A.; Bash, M.A.A.; Kadhim, M.J. Effect of plasma spray distance on the features and hardness reliability of YSZ thermal barrier coating. In Proceedings of the 3rd International Conference on Materials Engineering and Science (IConMEAS), Electr Network, Ho Chi Minh City, Vietnam, 6–8 January 2020; Elsevier: Amsterdam, The Netherlands, 2021.
25. Tamaki, R.; Yamakawa, M. Elucidation of Mechanism for Reducing Porosity in Electric Arc Spraying Through CFD. In Proceedings of the 18th International Conference on Computational Science (ICCS), Wuxi, China, 11–13 June 2018; Springer International Publishing Ag: Cham, Switzerland, 2018.
26. Hinners, H.; Konyashin, I.; Ries, B.; Petrzhik, M.; Levashov, E.A.; Park, D.; Weirich, T.; Mayer, J.; Mazilkin, A.A. Novel hardmetals with nano-grain reinforced binder for hard-facings. *Int. J. Refract. Met. Hard Mater.* **2017**, *67*, 98–104. [CrossRef]
27. Wang, Z.; Zhang, X.; Cheng, J.; Lin, J.; Zhou, Z. Cavitation Erosion Resistance of Fe-Based Amorphous/Nanocrystal Coatings Prepared by High-Velocity Arc Spraying. *J. Therm. Spray Technol.* **2014**, *23*, 742–749. [CrossRef]
28. Ashraf, M.A.; Ahmed, N.; Khan, Z.S.; Iqbal, M.A.; Satti, A.N.; Farooq, A. Effects of Annealing Treatment on Corrosion Resistance of Arc Sprayed Aluminum Coating. *J. Therm. Spray Technol.* **2022**, *31*, 1934–1943. [CrossRef]
29. Zhang, X.; Wang, Z.H.; Zhou, Z.H.; Lin, J.R. High Temperature Oxidation Behavior of Arc-sprayed FeCrBAlMo Coating. *J. Adv. Oxid. Technol.* **2016**, *19*, 105–112. [CrossRef]
30. Liang, X.-B.; Chen, Y.-X.; Zhang, Z.-B.; Wei, S.-C.; Guo, Y.-M.; Xu, B.-S. Research on automatic high velocity arc spraying technique and metastable coating materials. *Adv. Manuf.* **2013**, *1*, 97–101. [CrossRef]
31. Singh, H.; Prakash, S.; Puri, D. Some observations on the high temperature oxidation behaviour of plasma sprayed Ni_3Al coatings. *Mater. Sci. Eng. A* **2007**, *444*, 242–250. [CrossRef]
32. Morimoto, J.; Onoda, T.; Sasaki, Y.; Abe, N. Improvement of solid cold sprayed TiO_2–Zn coating with direct diode laser. *Vacuum* **2004**, *73*, 527–532. [CrossRef]